References and Notes

1. N. W. Ashcroft, N. D. Mermin, *Solid State Physics* (Brooks Cole, New York, 1976).
2. A. Y. Ganin *et al.*, *Nat. Mater.* **7**, 367 (2008).
3. M. S. Nam, A. Ardavan, S. J. Blundell, J. A. Schlueter, *Nature* **449**, 584 (2007).
4. A. Comanac, L. De'Medici, M. Capone, A. J. Millis, *Nat. Phys.* **4**, 287 (2008).
5. M. Capone, M. Fabrizio, C. Castellani, E. Tosatti, *Rev. Mod. Phys.*, in press; http://arxiv.org/abs/0809.0910 (2008).
6. M. Capone, M. Fabrizio, C. Castellani, E. Tosatti, *Science* **296**, 2364 (2002).
7. O. Gunnarsson, E. Koch, R. M. Martin, *Phys. Rev. B* **54**, R11026 (1996).
8. O. Gunnarsson, *Rev. Mod. Phys.* **69**, 575 (1997).
9. K. Tanigaki *et al.*, *Nature* **352**, 222 (1991).
10. P. Dahlke, M. S. Denning, P. F. Henry, M. J. Rosseinsky, *J. Am. Chem. Soc.* **122**, 12352 (2000).
11. T. T. M. Palstra *et al.*, *Solid State Commun.* **93**, 323 (1995).
12. S. Saito, K. Umemoto, S. G. Louie, M. L. Cohen, *Solid State Commun.* **130**, 335 (2004).
13. See supporting material on *Science* Online.
14. C. P. Schlicter, *Principles of Magnetic Resonance* (Springer, Heidelberg, 1990).
15. C. H. Pennington, V. A. Stenger, *Rev. Mod. Phys.* **68**, 855 (1996).
16. N. Sato *et al.*, *Phys. Rev. B* **58**, 12433 (1998).
17. K. Prassides *et al.*, *J. Am. Chem. Soc.* **121**, 11227 (1999).
18. G. R. Darling, A. Y. Ganin, M. J. Rosseinsky, Y. Takabayashi, K. Prassides, *Phys. Rev. Lett.* **101**, 136404 (2008).
19. O. Gunnarsson, J. E. Han, E. Koch, V. H. Crespi, *Struct. Bonding* **114**, 71 (2005).
20. T. Kambe, K. Kajiyoshi, M. Fujiwara, K. Oshima, *Phys. Rev. Lett.* **99**, 177205 (2007).
21. L. F. Chibotaru, *J. Mol. Struct.* **838**, 53 (2007).
22. T. Kawamoto, *Solid State Commun.* **101**, 231 (1997).
23. J. Curely, *Monatsh. Chem.* **136**, 987 (2005).
24. S. Margadonna, K. Prassides, H. Shimoda, T. Takenobu, Y. Iwasa, *Phys. Rev. B* **64**, 132414 (2001).
25. A. Y. Ganin *et al.*, *J. Am. Chem. Soc.* **128**, 14784 (2006).
26. Y. Takabayashi, A. Y. Ganin, M. J. Rosseinsky, K. Prassides, *Chem. Commun.* **2007**, 870 (2007).
27. Y. Iwasa, T. Takenobu, *J. Phys. Condens. Matter* **15**, R495 (2003).
28. Y. Iwasa, T. Kaneyasu, *Phys. Rev. B* **51**, 3678 (1995).

29. We thank the UK Engineering and Physical Sciences Research Council for funding under EP/C511794 and GR/S77820 and for access to the synchrotron x-ray facilities at the European Synchrotron Radiation Facility (where we thank A. N. Fitch for assistance on beamline ID31) and to the muon facilities at ISIS (where we thank S. R. Giblin for assistance on the MuSR instrument). We also thank SPring-8 for access to the synchrotron x-ray facilities.

Supporting Online Material

www.sciencemag.org/cgi/content/full/323/5921/1585/DC1
Materials and Methods
Figs. S1 to S4
References

1 December 2008; accepted 2 February 2009
10.1126/science.1169163

Omnidirectional Printing of Flexible, Stretchable, and Spanning Silver Microelectrodes

Bok Y. Ahn,[1,2] Eric B. Duoss,[1,2] Michael J. Motala,[1,3] Xiaoying Guo,[1,2] Sang-Il Park,[1,2] Yujie Xiong,[1,2] Jongseung Yoon,[1,2] Ralph G. Nuzzo,[1,3] John A. Rogers,[1,2,3] Jennifer A. Lewis[1,2]*

Flexible, stretchable, and spanning microelectrodes that carry signals from one circuit element to another are needed for many emerging forms of electronic and optoelectronic devices. We have patterned silver microelectrodes by omnidirectional printing of concentrated nanoparticle inks in both uniform and high–aspect ratio motifs with minimum widths of approximately 2 micrometers onto semiconductor, plastic, and glass substrates. The patterned microelectrodes can withstand repeated bending and stretching to large levels of strain with minimal degradation of their electrical properties. With this approach, wire bonding to fragile three-dimensional devices and spanning interconnects for solar cell and light-emitting diode arrays are demonstrated.

Printed electronics offer an attractive alternative to conventional technologies by enabling the creation of large-area, flexible devices at low cost (*1*). Although there are options available for electronic materials—including conducting polymers (*2*, *3*), inorganic semiconductors (*4*, *5*) and carbon nanotubes (*6*, *7*)—the ability to print low-resistance electrodes with fine resolution in high–aspect ratio layouts, and possibly spanning three dimensions, is a technologically important goal. Many applications, including solar cell metallization (*8*), flexible displays (*9*), radio frequency identification tags (*10*), and antennas (*11*), would benefit from this capability. Conventional approaches, such as screen-printing (*12*) and inkjet printing (*13*), produce low–aspect ratio features that must be supported by the underlying substrate or device, making it impossible to pattern spanning elements in- or out-of-plane.

Direct ink writing offers an attractive alternative for meeting the demanding design rules and form factors required for metallic electrodes in printed electronic and optoelectronic devices. In this filamentary printing approach, a concentrated ink is extruded through a tapered cylindrical nozzle that is translated using a three-axis, motion-controlled stage with nanoscale precision (Fig. 1A) (*14*). Yet, several limitations remain to be overcome. To date, the minimum feature size obtained with the use of nanoparticle inks is 100 μm (*15*). In addition, the inks had to be deposited in a non-wetting oil reservoir to avoid nozzle clogging. Finally, ink deposition has been confined solely to the *xy* plane, such that three-dimensional (3D) structures are assembled in a layerwise sequence. We report the omnidirectional printing of flexible, stretchable, and spanning microelectrodes using concentrated silver nanoparticle inks that readily flow through micronozzles in air.

Metallic nanoparticles are typically synthesized in solution by the reduction of metal precursors in the presence of surface capping agents (*16*–*19*). Through a multistep approach (fig. S1), we prepared highly concentrated silver nanoparticle inks using an aqueous system that contains silver nitrate as the silver precursor, poly(acrylic acid) (PAA) as the capping agent, and diethanolamine as the reducing agent (*20*, *21*). The components are first mixed under ambient conditions to create a population of very fine (~5-nm) silver nanoparticles. This particle

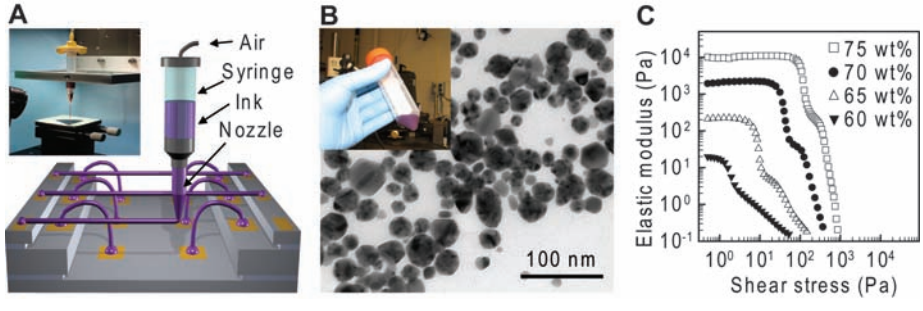

Fig. 1. (**A**) Schematic diagram illustrating omnidirectional printing and optical image of apparatus used (inset). (**B**) Transmission electron microscopy image of the synthesized silver nanoparticles and optical image of the concentrated ink (inset). (**C**) Shear elastic modulus as a function of shear stress for silver nanoparticle inks of varying solids loading.

[1]Frederick Seitz Materials Research Laboratory, University of Illinois at Urbana-Champaign, Urbana, IL 61801, USA. [2]Department of Materials Science and Engineering, University of Illinois at Urbana-Champaign, Urbana, IL 61801, USA. [3]Department of Chemistry, University of Illinois at Urbana-Champaign, Urbana, IL 61801, USA.

*To whom correspondence should be addressed. E-mail: jalewis@illinois.edu

population is ripened by heating the solution to 60°C (Fig. 1B). Ethanol, a poor solvent for the PAA-coated nanoparticles, is added to induce rapid particle coagulation. Next, the ink is centrifuged to achieve the desired solids loading [≥70 weight percent (wt %) silver nanoparticles], as shown in the inset of Fig. 1B. Finally, ethylene glycol is added as a humectant, which allows the ink to be patterned in air without clogging.

We have synthesized a broad range of silver nanoparticle inks and found that those with a solids loading between 70 and 85 wt %, a mean particle size of 20 ± 5 nm, and a particle size distribution between 5 and 50 nm exhibited both optimal flow behavior through fine deposition nozzles (1 to 30 μm) and low resistivity at modest annealing temperatures (≥200°C). Figure 1C shows the elastic modulus (G') as a function of shear stress for silver nanoparticle inks of varying solids loading. In the linear viscoelastic region, G' rises nearly three orders of magnitude as the nanoparticle content increases from 60 to 75 wt %. A minimum G' of 2000 Pa is required to produce spanning features, which occurs at a silver nanoparticle concentration of ~70 wt %. These highly concentrated inks can be stored under ambient conditions for weeks without any noticeable change in printing behavior (fig. S2).

To demonstrate the printing technique, we have patterned planar microelectrode arrays onto a silicon wafer by depositing silver nanoparticle ink (71–wt % solids) through 1-, 5-, and 10-μm cylindrical nozzles (Fig. 2A). Printed features with aspect ratios (h/w, where h is height and w is width) of ~0.7 are obtained in a single-pass, and a minimum width of ~2 μm is achieved with the use of a 1-μm nozzle. In addition, high–aspect ratio features are patterned in a layerwise manner, and their width and height are defined solely by the nozzle diameter and number of printed layers, respectively (Fig. 2, B and C).

The microstructural evolution of the printed silver microelectrodes as a function of annealing temperature is shown in Fig. 2D. As the temperature increases from 150° to 550°C, the microelectrodes undergo simultaneous loss of organics, grain growth, and densification. Thermogravimetic analysis reveals that the organic species are removed by ~400°C (fig. S1), whereas scanning electron microscopy (SEM) shows that their average grain size increases from ~180 nm at 150°C to 3 μm at 550°C, as a total volumetric shrinkage of ~30% occurs. Concomitantly, their electrical resistivity, ρ, decreases sharply over this temperature range (Fig. 2E). Upon annealing at 250°C for short times (≤30 min), the patterned microelectrodes exhibit an electrical resistivity of 5.2×10^{-5} ohm·cm, approaching the value of bulk silver (10^{-6} ohm·cm). In contrast, microelectrodes annealed at 150°C require several hours (≥25 hours) to reach $\rho \sim 10^{-3}$ ohm·cm, a value comparable to that observed for doped poly(3,4-ethylenedioxythiopene)/poly(styrenesulfonate), a widely used organic conductor (*22*, *23*).

To demonstrate the flexibility of the printed features, we patterned a series of interdigitated microelectrode arrays on a polyimide substrate. Figure 3A shows optical and SEM images of the printed silver microelectrodes after annealing at 200°C for 3 hours, followed by wrapping the patterned substrate around a scintillation vial with a bending radius of 14 mm. Solid contact pads (1 by 1 mm) connected to linear electrode features are formed with a 30-μm nozzle, to which interdigitated features are patterned with a 5-μm nozzle (Fig. 3A, top right). These elaborate structures require the initiation and cessation of ink flow multiple times during the printing process (Fig. 3A, bottom right).

To investigate the effects of mechanical bending on electrical performance, we used a custom-built mechanical stage coupled to a micropositioner to carry out bend tests (fig. S3A). For this experiment, a linear array of 10 silver microelectrodes (w = 23 μm, h = 12 μm, and length l = 1 cm) spaced 0.5 mm apart are printed on a 25-μm-thick polyimide sheet and annealed at 200°C for 3 hours in air before mechanical testing. Their electrical resistivity is measured as a function of bending radius from ±11 mm to ±5 mm, and the reported ρ values are averaged from 10 electrodes. In the first bend cycle, ρ is found to be $6.23 \pm 4.40 \times 10^{-4}$, $2.11 \pm 0.91 \times 10^{-4}$, and $2.00 \pm 1.11 \times 10^{-4}$ ohm·cm in tension (convex), unstrained (flat), and compression (concave), respectively (Fig. 3B). An approximately twofold change in electrical resistivity is observed after 1000 bend cycles at the smallest radius of ±5 mm (Fig. 3C), where $(\rho_{1000} - \rho_0)/\rho_0$ is 2.17, 1.66, and 1.67 for the tensile, unstrained, and compressive states, respectively, and ρ_0 is the initial value measured in the unstrained state. The microelectrodes exhibited robust response for at least 750 bending cycles.

Ultrathin (~20 nm) metal films deposited onto prestrained, stretchable substrates can form wavy buckles and arches upon relaxation of the substrate (*24*). These configurations are even observed in brittle semiconductor materials, such as silicon, because of the differences in mechanical behavior between ultrathin and bulk materials (*25*). The built-in slack enables mechanical stretching while preserving the desired electronic properties. Stretchable, wavy, and arched architectures can also be created out of nonbrittle materials that are not ultrathin, particularly for ductile metals. Figure 3D shows stretchable silver arches formed by printing a spanning silver microelec-

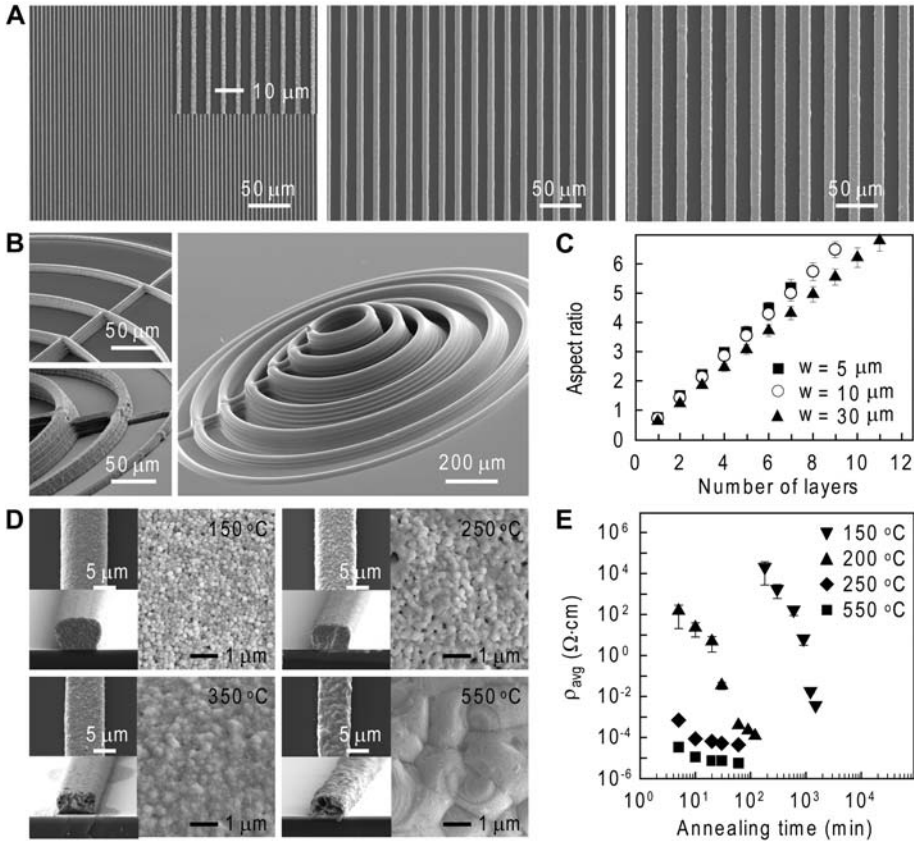

Fig. 2. (**A**) SEM images of planar arrays of silver microelectrodes patterned with 1- (left), 5- (center), and 10-μm (right) nozzles. (**B**) SEM images of multilayer silver microelectrodes patterned with 5- (top left), 10- (bottom left), and 30-μm (right) nozzles. (**C**) Aspect ratio as a function of number of printed layers for the silver microelectrodes shown in Fig. 2B. (**D**) SEM images of silver microelectrodes patterned with a 15-μm nozzle as a function of annealing temperature. (**E**) Electrical resistivity of silver microelectrodes as a function of annealing temperature and time. Error bars indicate the SD measured from three electrodes.

trode onto a prestrained spring (inset) that is then released to form the desired arches. The specimens are annealed at varying temperatures, and a silicone adhesive is subsequently printed onto the spring at the microelectrode contact points to ensure good adhesion and accurate resistivity measurements. The electrical resistivity of the silver microelectrode arches annealed at different temperatures is plotted as a function of strain $[(L - L_0)/L_0 \times 100\%]$ in Fig. 3E. The maximum strain increases with increasing annealing temperature from 8% at 200°C to 25% at 550°C, as the microelectrodes transform to a bulklike ductility. Straining these microelectrodes up to 200 cycles does not result in fatigue-induced failure at the contact points (Fig. 3F).

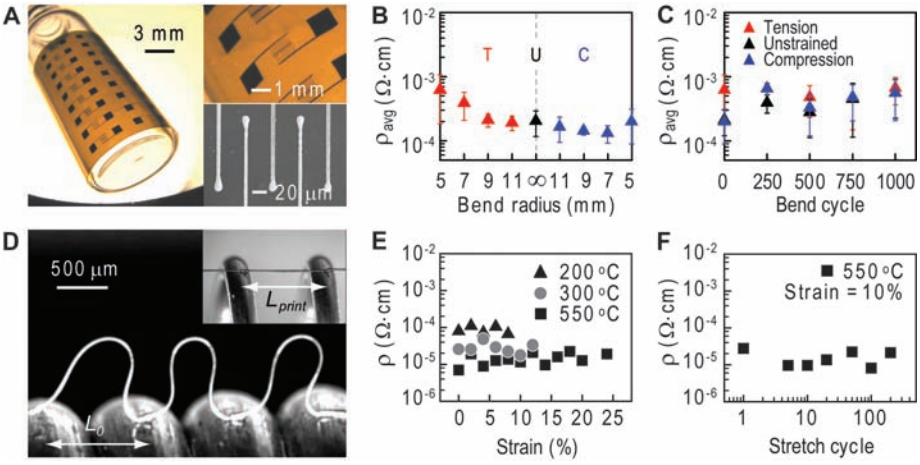

Fig. 3. (**A**) Optical and SEM images of silver microelectrodes patterned on a polyimide substrate with a bend radius of 14 mm. (**B**) Electrical resistivity of the silver microelectrodes as a function of bend radius under tension (T), unstrained (U), and compression (C). (**C**) Electrical resistivity of the silver microelectrodes as a function of bend cycle at a bend radius of ±5 mm. (**D**) Optical image of stretchable silver arches printed onto a spring. (**E**) Electrical resistivity of the stretchable silver microelectrode arches as a function of strain and annealing temperature. (**F**) Electrical resistivity of the stretchable silver microelectrode arches as a function of strain cycle. Error bars indicate the SD measured from 10 electrodes.

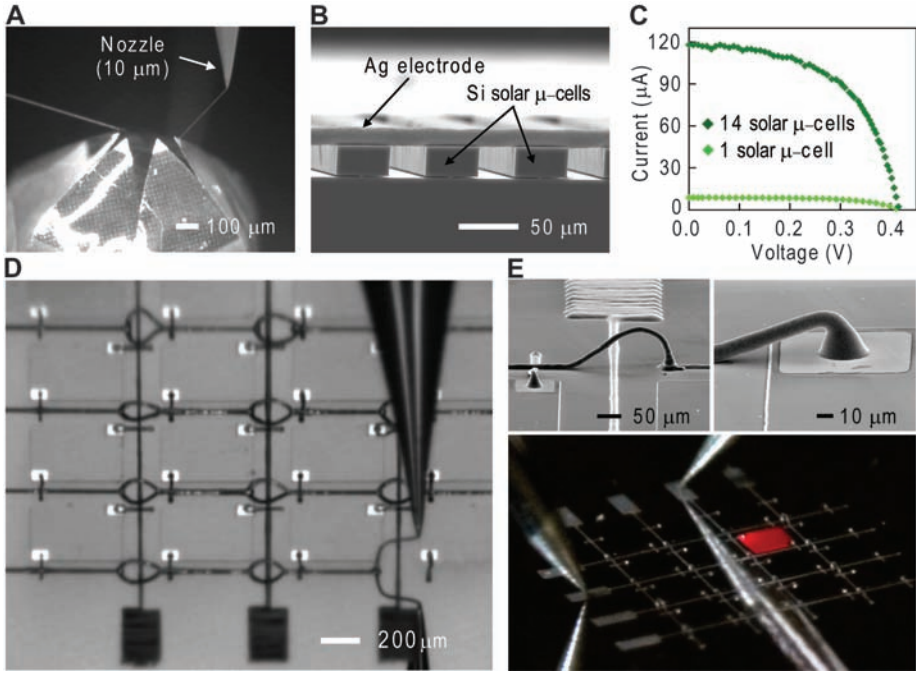

Fig. 4. (**A**) Optical image obtained during wire bonding onto a thin (2-μm) silicon spherical shell using a 10-μm nozzle. (**B**) Optical image of a spanning silver microelectrode printed onto an unplanarized, silicon solar microcell array. (**C**) Current (*I*)–voltage (*V*) response of an individual silicon solar microcell and a 14-microcell array connected by silver microelectrodes. (**D**) Optical image acquired during patterning of silver interconnects on a gallium arsenide–based, 4-by-4 LED chip array. (**E**) A silver interconnect arch printed over an electrode junction (top left) and on a gold contact pad (80 by 80 μm) (top right) and an optical image of light emission from a single LED pixel in the $y = 2$, $x = 3$ position within the array under an applied voltage (bottom).

We have provided a few examples of conductive features that can be patterned across unsupported regions in three dimensions. It is possible to vertically print microelectrodes with arbitrary height and angle (fig. S4). Figure 4A shows wire bonding of silver microelectrodes onto the surface of a thin silicon spherical shell assembled by lithographically patterning, releasing, and folding a 2-μm silicon layer in the desired 3D form (fig. S5). Unlike conventional techniques (*26*), our approach allows fine silver microwires (~10 μm) to be bonded with minimal contact pressure on both flat and curved surfaces, which is highly advantageous for delicate devices.

When combined with other processes (for instance, photolithography and transfer printing), our ink writing technique enables the heterogeneous integration of dissimilar materials (*8*, *27*). To further highlight this capability, we have patterned interconnects for both solar microcell and light-emitting diode (LED) arrays. As a first example, we patterned silver microelectrodes (w = 15 μm, h = 13 μm) onto a silicon solar microcell (w = 45 μm, h = 26 μm, and l = 2 mm) array, in which each photovoltaic element is separated by a 33-μm gap (fig S6). Figure 4B shows that the silver microelectrodes span the unsupported regions between each solar microcell without deformation. We also find that these inks can span unsupported gaps that are extraordinarily wide, up to 1.0 cm across (fig. S7). The current (*I*)–voltage (*V*) response from an individual silicon solar microcell and 14 interconnected microcells under a simulated air mass 1.5 illumination condition of 1000 W·m^{-2} is shown in Fig. 4C. Because of their fine lateral dimensions, these conductive tracks can be spaced closely together, thereby blocking less incoming light and allowing more current to be drawn from each solar cell (*28*).

As a final demonstration, we exploited omnidirectional printing to create interconnects for the gallium arsenide–based LED array (4-by-4 pixels, where each pixel is 500 by 500 by 2.5 μm and spaced 200 μm apart) shown in Fig. 4D. The ability to print out-of-plane enables the microelectrodes to directly cross pre-existing patterned features through the formation of spanning arches (Fig. 4E, top left). Typically, insulating layers or bypass electrode arrays are required in conventional layouts. Figure 4E (top right) shows silver micro-arches printed on a gold pad (80 by 80 μm) on a LED pixel. Figure 4E (bottom) displays the LED array, emitting uniform red light under an applied bias of 6 V from a single pixel, after annealing at 200°C for 3 hours. The utility of this approach is further established by printing spanning arches onto commercially available gallium nitride LED chips (fig. S8).

In summary, we have demonstrated the omnidirectional printing of flexible, stretchable, and spanning microelectrodes with the use of tailored silver nanoparticle inks. By carefully controlling

the silver nanoparticle concentration, size, and distribution, we have produced inks with high solids loading (≥70 wt %) that are ideally suited for direct-write assembly. We have shown that self-supporting microelectrodes in either planar or 3D forms of arbitrary complexity can be patterned on a wide variety of substrates. Using this technique, we have further demonstrated the feasibility of wire bonding to fragile devices and patterning complex interconnects for solar cell and LED arrays.

References and Notes

1. D. B. Chrisey, *Science* **289**, 879 (2000).
2. H. Sirringhaus *et al.*, *Science* **290**, 2123 (2000).
3. S. R. Forrest, *Nature* **428**, 911 (2004).
4. Y. Sun, J. A. Rogers, *Adv. Mater.* **19**, 1897 (2007).
5. E. Menard *et al.*, *Chem. Rev.* **107**, 1117 (2007).
6. M. C. LeMieux *et al.*, *Science* **321**, 101 (2008).
7. Q. Cao *et al.*, *Nature* **454**, 495 (2008).
8. J. Yoon *et al.*, *Nat. Mater.* **7**, 907 (2008).
9. J. A. Rogers *et al.*, *Proc. Natl. Acad. Sci. U.S.A.* **98**, 4835 (2001).
10. V. Subramanian *et al.*, *Proc. IEEE* **93**, 1330 (2005).
11. R. A. Potyrailo, W. G. Morris, *Anal. Chem.* **79**, 45 (2007).
12. M. Hosokawa, K. Nogi, M. Naito, T. Yokoyama, *Nanoparticle Technology Handbook* (Elsevier, Oxford, ed. 1, 2007).
13. T. H. J. van Osch, J. Perelaer, A. W. M. de Laat, U. S. Schubert, *Adv. Mater.* **20**, 343 (2008).
14. J. E. Smay, J. Cesarano III, J. A. Lewis, *Langmuir* **18**, 5429 (2002).
15. Q. Li, J. A. Lewis, *Adv. Mater.* **15**, 1639 (2003).
16. Y. Sun, Y. Xia, *Science* **298**, 2176 (2002).
17. B. Wiley, Y. Sun, Y. Xia, *Acc. Chem. Res.* **40**, 1067 (2007).
18. M. Yamamoto, Y. Kashiwagi, M. Nakamoto, *Langmuir* **22**, 8581 (2006).
19. A. Pyatenko, M. Yamaguchi, M. Suzuki, *J. Phys. Chem. C* **111**, 7910 (2007).
20. B.-H. Ryu *et al.*, *Colloids Surf. A Physicochem. Eng. Asp.* **270–271**, 345 (2005).
21. Materials and methods are available as supporting material on *Science* Online.
22. M. Dobbelin *et al.*, *Chem. Mater.* **19**, 2147 (2007).
23. J. Ouyang *et al.*, *Polymer* **45**, 8443 (2004).
24. T. Li, Z. Huang, Z. Suo, S. P. Lacour, S. Wagner, *Appl. Phys. Lett.* **85**, 3435 (2004).
25. D.-Y. Khang, H. Jiang, Y. Huang, J. A. Rogers, *Science* **311**, 208 (2006); published online 14 December 2005 (10.1126/science.1121401).
26. G. G. Harman, *Wire Bonding in Microelectronics: Process, Reliability, and Yield* (McGraw-Hill Professional, New York, 1997).
27. J.-H. Ahn *et al.*, *Science* **314**, 1754 (2006).
28. S. Ashley, *Sci. Am.* **299**, 32 (2008).

29. This material is based on work supported by the U.S. Department of Energy, Materials Sciences and Engineering Division under award no. DEFG-02-07ER46471, through the Frederick Seitz Materials Research Laboratory (FSMRL) at the University of Illinois. The authors gratefully acknowledge use of the FSMRL Central Facilities, including Center for Microanalysis of Materials. B.Y.A. thanks the Korean Research Foundation for the postdoctoral fellowship. We also thank C. Hansen, M. Xu, R. Shepherd, J. Bukowski, J. Carroll III, and J. Yoshikawa for useful discussions. J.A.L., B.Y.A., and E.B.D. submitted a U.S. patent application on this work entitled "Metal Nanoparticle Inks" on 3 October 2008.

Supporting Online Material

www.sciencemag.org/cgi/content/full/1168375/DC1
Materials and Methods
Figs. S1 to S9
References

11 November 2008; accepted 27 January 2009
Published online 12 February 2009;
10.1126/science.1168375
Include this information when citing this paper.

A Meta-Selective Copper-Catalyzed C–H Bond Arylation

Robert J. Phipps and Matthew J. Gaunt*

For over a century, chemical transformations of benzene derivatives have been guided by the high selectivity for electrophilic attack at the ortho/para positions in electron-rich substrates and at the meta position in electron-deficient molecules. We have developed a copper-catalyzed arylation reaction that, in contrast, selectively substitutes phenyl electrophiles at the aromatic carbon–hydrogen sites meta to an amido substituent. This previously elusive class of transformation is applicable to a broad range of aromatic compounds.

Aromatic organic compounds are ubiquitous in modern society as medicines and functionalized materials (*1*). These molecules comprise cyclic aryl cores with an often complex array of substituents on the ring carbons, which in many cases are most straightforwardly appended by electrophilic substitution (*2*). Ever since the pioneering work of Friedel and Crafts (*3*), it has been widely established that electron-donating substituents direct incoming electrophiles to the ortho and para positions, whereas electron-withdrawing groups steer to the meta position (Fig. 1A). This fundamental reactivity pattern facilitates a predictable outcome in simple cases; however, a common problem encountered in synthesis is how to access the isomer that is not anticipated by these rules. Solutions to this problem often require numerous functional group additions or manipulations in order to tailor the directing electronic properties of the precursor to furnish the desired product. Furthermore, in complex systems, where there may be more than one electronic or sterically active substituent, the competition between these directing groups may lead to mixtures of products. Although there have been some reports that indirectly address these problems (*4*–*7*), circumventing the inherent ortho/para-selectivity of electron-rich aromatic systems to generate the meta product remains a largely elusive and unmet goal for chemical synthesis.

A central theme of our research has been the development of methods to obviate reliance on complex functional group manipulations through direct metal-catalyzed C–H bond transformations (*8*, *9*). A key aspect of this goal is the ability to control the site selectivity of these transformations under mild conditions; a challenge that is further complicated by the ubiquitous nature of the C–H bond in organic molecules (*10*–*15*). The three mechanisms that usually rationalize the majority of selective metal-catalyzed C–H bond activation methods involve electrophilic aromatic substitution with electron-rich, π-nucleophilic arenes (*16*), concerted metalation-deprotonation with simple and electron-deficient benzenes (*17*–*19*), and directed cyclometalation (*20*–*26*). These mechanistic pathways most commonly form the ortho-substitution product, and as a result there is a paucity of methods for metal-catalyzed C–H bond activation at the meta position of a substituted benzene ring (*27*, *28*).

Here we describe the development of a reactivity concept for a metal-catalyzed aromatic C–H bond functionalization strategy that selectively generates the elusive meta isomer. The outcome is not predicted by the conventional rules associated with electronic factors, directing groups, or steric effects, and provides direct access to the meta isomer on highly versatile electron-rich aromatic structures. The process is simple, proceeds under mild conditions, uses inexpensive copper catalysts, and forms valuable products that would be difficult to synthesize by other methods (Fig. 1B). Furthermore, the reactivity and selectivity of this process should be compatible with other arene and C–H bond transformations and will streamline synthetic strategy for the assembly of medicines, natural products, and industrially relevant aromatic molecules.

We previously identified a copper catalysis system, based on electrophilic metalation, that enables site-selective C–H bond arylation on the indole skeleton (Fig. 2A) (*10*). We speculated that a Cu(I) catalyst is oxidized to a Cu(III)-aryl intermediate (*29*), a highly electrophilic d^8-configured metal species, that undergoes Friedel-Crafts–type metalation and arylation at the C3 position of the indole (Fig. 2B). We see C3 arylation when using our copper catalyst, whereas an almost identical process using Pd(II)-salts delivers the C2 isomer (*30*). Although the origin of this dichotomy remains unclear, it led us to speculate that use of our copper catalyst might enable us to reverse the established selectivity of other electrophilic Pd(II)-catalyzed transformations. For example, many Pd(II)-catalyzed reactions are ortho-selective and have been routinely developed by virtue of the coordinat-

Department of Chemistry, University of Cambridge, Lensfield Road, Cambridge CB2 1EW, UK.

*To whom correspondence should be addressed. E-mail: mjg32@cam.ac.uk